JOURNAL OF NEUROTRAUMA 27:1–12 (November 2010)

DOI: 10.1089/neu.2010.1345

Spinal Cord Blood Flow and Blood Vessel Permeability Measured by Dynamic Computed Tomography Imaging in Rats after Localized Delivery of Fibroblast Growth Factor

Catherine E. Kang,[1,2] Richard Clarkson,[3] Charles H. Tator,[4] Ivan W.T. Yeung,[3,5] and Molly S. Shoichet[1,2,6]

Abstract

Following spinal cord injury, profound vascular changes lead to ischemia and hypoxia of spinal cord tissue. Since fibroblast growth factor 2 (FGF2) has angiogenic effects, its delivery to the injured spinal cord may attenuate the tissue damage associated with ischemia. To limit systemic mitogenic effects, FGF2 was delivered to the spinal cord via a gel of hyaluronan and methylcellulose (HAMC) injected into the intrathecal space, and compared to controls receiving HAMC alone and artificial cerebrospinal fluid (aCSF) alone. Dynamic perfusion computed tomography (CT) was employed for the first time in small animals to serially measure blood flow and permeability in the injured and uninjured spinal cord. Spinal cord blood flow (SCBF) and permeability-surface area (PS) measurements were obtained near the injury epicenter, and at two regions rostral to the epicenter in animals that received a 26-g clip compression injury. As predicted, SCBF measurements decreased and PS increased after injury. FGF2 delivered via HAMC after injury restored SCBF towards pre-injury values in all regions, and increased blood flow rates at 7 days post-injury compared to pre-injury measurements. PS was stabilized at regions rostral to the epicenter of injury when FGF2 was delivered with HAMC, with significantly lower values than aCSF controls at 7 days in the region farthest from the epicenter. Laminin staining for blood vessels showed a qualitative increase in vessel density after 7 days when FGF2 was locally delivered. Additionally, permeability stains showed that FGF2 moderately decreased permeability at 7 days post-injury. These data demonstrate that localized delivery of FGF2 improves spinal cord hemodynamics following injury, and that perfusion CT is an important technique to serially measure these parameters in small animal models of spinal cord injury.

Key words: blood flow; growth factors; computed tomography scanning; traumatic spinal cord injury

Introduction

Traumatic spinal cord injury (SCI) is a serious condition that often causes paralysis and severe loss of function. A recent study showed that more than 1.2 million people in the U.S. report being paralyzed due to SCI, and nearly 50% of those people reported "a lot of difficulty in movement" or "a complete inability to move" (Reeve Foundation, 2009). Pharmacotherapy for acute SCI is currently limited to intravenous administration of the steroid methylprednisolone; however, its efficacy in improving functional recovery has been questioned (Fehlings, 2001). The early secondary events seen following the initial spinal cord trauma lead to rapid and profound tissue changes, including hemorrhage, inflammation, edema, and ischemia, all of which have significant impact on tissue and functional recovery. Several drug treatments using systemic delivery are designed to target and limit these secondary injury mechanisms, and have undergone clinical trials (Hawryluk et al., 2008; Tator, 2006); however, none has shown sufficient improvement in human functional recovery to become established as standard clinical practice. Re-establishing blood flow to the injured tissue could have a neuroprotective effect by limiting the degeneration resulting from ischemia.

[1]Department of Chemical Engineering and Applied Chemistry, [5]Department of Radiation Oncology, and [6]Department of Chemistry, University of Toronto, Toronto, Ontario, Canada.
[2]Institute of Biomaterials and Biomedical Engineering, Toronto, Ontario, Canada.
[3]Department of Radiation Physics, Princess Margaret Hospital, University Health Network, Toronto, Ontario, Canada.
[4]Krembil Neuroscience Centre, Toronto Western Research Institute, and Department of Surgery, University of Toronto, Toronto, Ontario, Canada.

Fibroblast growth factor 2 (FGF2) has been shown to both promote angiogenesis (Montesano et al., 1986; Relf et al., 1997; Shing et al., 1985), and to be neuroprotective (Lee et al., 1999; Nozaki et al., 1993). *Ex vivo* studies suggest that FGF2 reduces permeability of the damaged blood–brain barrier (Bendfeldt et al., 2007; Reuss et al., 2003). *In vivo* studies demonstrate that FGF2 enhances functional recovery in spinal-cord-injured rats when delivered locally via an osmotic minipump (Rabchevsky et al., 1999, 2000). Thus we hypothesized that FGF2 can improve spinal cord blood flow (SCBF) and reduce permeability following injury, yet requires a local delivery strategy because it does not cross the blood–spinal cord barrier (BSCB) (Relf et al., 1997). While systemic drug delivery is the most common practice clinically, it requires that molecules cross the BSCB, and high doses are necessary to reach therapeutic levels at the site of injury, often leading to undesirable side effects. Drug delivery systems have been designed to circumvent these limitations, such as bolus intrathecal delivery and implantable catheters/minipump devices. However, these systems are either transient, or can cause complications such as infection (Jones and Tuszynski, 2001). To overcome these limitations, our lab has developed a minimally-invasive, intrathecal drug delivery system that is safe for local delivery of therapeutic agents to the site of injury (Gupta et al., 2006; Kang et al., 2009a). This localized delivery system, composed of a biopolymer blend of hyaluronan and methylcellulose (HAMC), is injected into the intrathecal space and locally releases FGF2 into the injured spinal cord for at least 6 h (Kang et al., 2009b).

In order to evaluate the potential benefit of local FGF2 delivery via HAMC to the injured spinal cord, a dynamic method to serially study hemodynamics in the same animal over time was required. Early work in cerebral blood flow using gas clearance techniques has been well characterized and modeled by Kety and Schmidt, based on Fick's principles of diffusion (Kety and Schmidt, 1948; Kety, 1951). In this method, an inhalable and inert gas to which the BSCB is completely permeable is first allowed to permeate the tissues until saturation, and the clearance of the gas is then measured by electrodes placed within the tissue as a function of time to determine the flow rate. Although very useful for dynamically measuring blood flow, tissue damage occurs from the probes that are inserted into the tissue for measurement. Other methods for measuring SCBF, such as autoradiography, require a timed infusion of a radioisotope and subsequent sectioning of the tissue (Sandler and Tator, 1976). The radioisotope is detected in tissue sections and quantified using densitometry to assess regional flow into grey and white matter in the spinal cord. Indicator fractionation techniques are similar, but instead use labeled microparticles in place of a radioisotope (Sandler and Tator, 1976). More recently, the laser Doppler technique has been used, but since it requires the probe to be on the surface of the spinal cord, it is limited to either a relatively short time frame after the animal has undergone the injury, or a terminal time point (Toda et al., 2008).

Magnetic resonance imaging (MRI) and computed tomography (CT) now have improved resolution, and when combined with dynamic contrast enhancement (DCE), blood flow and permeability can be measured as contrast agents are injected into the bloodstream (Bisdas et al., 2008; Leggett et al., 1998; Miles, 1991; Miles et al., 1993, 1998, 2000; Tateishi et al., 2001; Yeung et al., 1994; Yi et al., 2004). With MRI and CT, gadolinium-chelates and iodinated contrast agents, respectively, can be introduced into the bloodstream and the perfusion rate measured as they pass through the tissues. Because these contrast agents or tracers do not diffuse freely into the tissue as gases would, tracer movement into the tissue is measured rather than clearance out of the tissue, as is done using Kety-Schmidt principles. Both MRI and CT have been used for dynamic measurements, though multi-detector CT machines can achieve better temporal and spatial resolution than MRI. Additionally, at very high spatial resolutions, MRI is often susceptible to more motion artifacts than CT. Thus we pursued CT as a method for dynamic measurements within the spinal cord. The use of contrast agents with CT imaging is known as dynamic perfusion CT or DCE CT, and this method has been used in several applications in both animal and human studies. Initially, the method was used to investigate renal blood flow (Miles, 1991; Peters et al., 1987a, 1987b), but further technical developments allowed measurements of tumor blood flow in cerebral tumors (Leggett et al., 1998; Yeung et al., 1994), and lung cancers (Tateishi et al., 2001; Yi et al., 2004), as well as renal and hepatic metastases (Miles, 1991; Miles et al., 1993, 1998). A recent report discusses the first use of CT perfusion for SCBF in humans (Bisdas et al., 2008), but this technique has not yet been reported for small animals. In this article we evaluate dynamic CT imaging for repeated measurements of SCBF and permeability-surface area (PS) in rats after SCI, and with this technique assess the effect of local delivery of FGF2 via HAMC on SCBF and permeability of the injured spinal cord.

Methods

All chemicals were purchased from Sigma-Aldrich Chemical Co. (Mississauga, ON) and used as received unless otherwise noted.

Hyaluronan and methylcellulose preparation

First, 2 wt% hyaluronan and 7 wt% methylcellulose were prepared as previously described (Kang et al., 2009a). Briefly, sterile methylcellulose (13×10^3 Da) and sodium hyaluronate (1.5×10^6 Da; Novamatrix, Drammen, Norway) powders were sequentially dissolved in artificial cerebrospinal fluid (aCSF) in a laminar flow hood. The aCSF was prepared in dH_2O with 148 mM NaCl, 3 mM KCl, 0.8 mM $MgCl_2$, 1.4 mM $CaCl_2$, 1.5 mM Na_2HPO_4, and 0.2 mM NaH_2PO_4 (Jimenez Hamann et al., 2003). To distribute recombinant human FGF2 (Biovision, Mountain View, CA) in HAMC, a solution of 10 μg/mL of FGF2 dissolved in aCSF was used in place of aCSF alone in the procedure above. This resulted in 10 μg/mL FGF2 loaded into a 2% HA and 7% MC solution.

In vivo *surgical procedures*

All animal procedures were performed in accordance with the Guide to the Care and Use of Experimental Animals developed by the Canadian Council on Animal Care, and approved by the Animal Care Committee at the Research Institute of University Health Network. Twenty-four adult Sprague-Dawley rats (200–250 g; Charles River, Montreal, Quebec, Canada) purchased with implanted jugular vein catheters were anesthetized by inhalational isoflurane, and a laminectomy was performed at the T1–T2 vertebral level. The

animals were imaged with dynamic perfusion CT immediately following the laminectomy to obtain normal, pre-injury measurements. A modified aneurysm clip calibrated to a closing force of 26 g was applied to the spinal cord at T2 for 1 min to produce a moderate SCI as previously described (Rivlin and Tator, 1978). A durotomy was performed immediately caudal to the injury site with a 30-g bent beveled needle, and then a 30 g blunt bent-tipped needle was inserted through the durotomy into the intrathecal space. The animals received either 10 μL of aCSF ($n=8$), 10 μL of HAMC ($n=8$), or 10 μL of FGF2-loaded HAMC (10 μg/mL FGF2, $n=8$), through the needle that was then maintained in the intrathecal space for 1 min before removal to allow HAMC gelation in the intrathecal space (Gupta et al., 2006). Following injection, the overlying muscles and fascia were sutured, the rats were ventilated with pure oxygen, and then they were placed under a heat lamp for recovery. Buprenorphine was administered post-surgery for pain management. CT imaging was performed at this time to obtain immediate post-injury measurements, and serial imaging was performed at 1 d post-injury and 7 d post-injury in the same animals.

Computed tomography imaging acquisition with dynamic contrast enhancement

The animals were kept under isoflurane anesthesia for the duration of the CT scans, which were obtained with a MicroCT scanner (Locus Ultra MicroCT; GE Medical Systems, Milwaukee, WI) in the Spatio-Temporal Targeting and Amplification of Radiation Response Facility (Toronto, Ontario, Canada). A scout x-ray was performed to define the level of interest corresponding to approximately C5 through T4. A perfusion scan was then performed over the selected region, at an in-plane resolution of 0.15×0.15 mm with a slice thickness of 0.15 mm covering a range of z = 13.5 mm at an energy level of 60 kV and 90 mA. The iodinated contrast agent Visipaque™ (270 mg I/mL; GE Healthcare) was injected as the scan started by means of a foot-pedal-controlled injection pump (NE-1000 Single Syringe Programmable Pump; New Era Pump Systems, Inc., Farmingdale, NY). The contrast was warmed to 37°C to reduce viscosity, and was delivered in the first 10 sec of the scan at a rate of 124.2 mL/h (a total of 354 μL was delivered) through the implanted jugular catheter. A 3-min multiphase scan protocol was used, acquiring a volume every second for the first 30 sec, then every 10 sec for the remaining 150 sec.

Image analysis

Previous measurements of SCBF have been developed by Kety and Schmidt, using inert gases to which the BSCB is completely permeable. The intravascular space, *i*, and the extravascular space, *e*, are considered to be a single compartment, and rate constants for gas movement are equal between the extravascular and the intravascular spaces (k_{ei} and k_{ie} in Fig. 1A). SCBF is thus calculated by Eqn. (1) (Kety and Schmidt, 1948):

$$SCBF = \frac{\frac{dQ_{T(t)}/dt}{W_T}}{\int_0^t (C_A - C_V)dt} \quad (1)$$

where $Q_T(t)$ is the quantity of gas in tissue T at time t, W is the weight of the tissue, and the denominator is the difference between the arterial and venous curves for gas concentration over time. The CT technique used here builds on this model, but employs different assumptions and indicator techniques. Because the contrast agent is not very permeable to the BSCB, the intravascular and extravascular spaces within the tissue can be viewed separately (Fig. 1B), unlike models developed by Kety and Schmidt. A consensus paper by Tofts and associates (Tofts et al., 1999) describes this model in detail, known as the Modified Tofts Model, including the limitations under different conditions, and the association of fitting parameters to physiological parameters. In this two-compartment model, the tissue is composed of the intravascular and extravascular components, and a permeable tracer moves from the intravascular space to the extravascular space at a volume rate constant of K^{trans}. Because the tracer is sequestered in the plasma of the blood, the rate constant k_{ep} is defined as the rate of transport from the extravascular space to the plasma portion of the blood. The unidirectional transport of tracer is dependent on the permeability and the surface area of the endothelial layer that separates the intravascular and extravascular spaces in the selected region. Thus, this method calculates the product of permeability and surface area of endothelium in selected regions, known as the permeability-surface area product, or PS. The generalized kinetic model for two compartments as previously described by Tofts and associates (Tofts et al., 1999) is shown in Eqn. (2a):

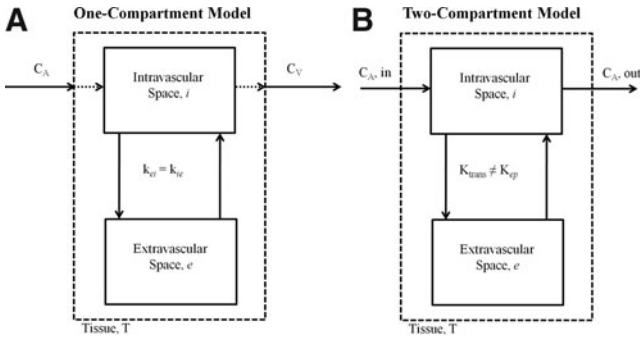

FIG. 1. (A) One-compartment and **(B)** two-compartment model of blood flow.

$$C_T(t) = K^{trans} \int C_p(\tau) e^{-k_{ep}(1-t)} d\tau \quad (2a)$$

and with the initial conditions that $C_p = C_T = 0$ at $t = 0$, this equation simplifies to:

$$\frac{dc_T}{dt} = K^{trans}(C_p - C_e) \quad (2b)$$

where C_p is the concentration in the plasma [defined as $C_a/(1–Hct)$ where Hct is the blood hematocrit], and C_e is the concentration in the extravascular space (defined as C_T/v_e, where v_e is the fractional volume of the extravascular space). This model can be used for any tissue, but the parameters will vary based on the assumptions applied to the system. In a flow-limited situation in which a tracer is very permeable across the endothelial layer (e.g., where $PS >> F$), the equation further simplifies to the Kety model shown in Eqn. (3), in

which contrast enhancement is related to flow (F) in the following manner:

$$\frac{dc_T}{dt} = F\rho(C_A - C_V) = F\rho(1 - Hct)(C_p - C_e) \quad (3)$$

where $C_A = C_p\ (1–Hct)$ and $C_V = (1–Hct)\ C_e$ (tissue density ρ is required since F is per unit mass of tissue). SCBF measurements made with the models developed by Kety have customarily been reported as milliliters per minute per 100 g of tissue rather than per 1 g of tissue, and this convention is maintained here to allow for comparison with previous work. In a permeability-limited situation, in which the tracer is not very permeable to the endothelial layer (e.g., where $F >> PS$) then the situation simplifies to Eqn. (4):

$$\frac{dc_T}{dt} = PS\rho(C_p - C_e) \quad (4)$$

where the units of PS are milliliters per minute per gram. Thus, in a flow-limited situation, $K^{trans} = F\rho\ (1–Hct)$ ($PS >> F$), and in a permeability-limited situation, $K^{trans} = PS\rho$ ($F >> PS$). In the central nervous system, the BSCB is mostly impermeable to many compounds, thus $F >> PS$ and the K^{trans} value can be used to estimate PS. Thus, Eqn. 4 was utilized in these studies to calculate PS values in the uninjured and injured spinal cord.

A simpler method for measuring F has been estimated from the first pass of an iodinated compound through the tissue, and flow is only dependent on the maximum amount flowing into the tissue shown in Eqn. (5) (Miles, 1991; Peters et al., 1987a, 1987b):

$$F\rho = \frac{(dc_T/dt)_{max}}{C_{A_{max}}} \quad (5)$$

where flow is equivalent to the ratio of the maximal slope of the tissue intensity curve and the peak height of the arterial curve. In this case, the perfusion rate through tissue is only depicting the perfusion of the intravascular component, ignoring the extravascular component. The underlying assumption is that in the short time used to measure peak tissue enhancement (usually done in the first 10 sec), an insignificant amount of the tracer has permeated into the tissue and thus can be ignored. This equation is only valid for cases in which the tracer is not extremely permeable to the membrane, and thus is measuring tracer uptake into the tissue rather than tracer washout. Therefore, Eqn. 5 was used to determine SCBF in the uninjured and injured spinal cord from the first pass of contrast through the tissue.

Post-processing of the CT images obtained was performed using the open source ClearCanvas Software (Toronto, Ontario, Canada), with a DCE tool developed at the University Health Network in Toronto, utilizing the Modified Toft's Model. A region of interest in the ascending aorta superior to the heart (at T3) was defined, and the time-intensity curve was produced for the arterial input function. A tissue region of interest for the spinal cord was then defined using average spinal cord measurements for the long and short axes of the spinal cord at each vertebral level (Hebel and Stromberg, 1986), and using the remaining portions of the vertebrae as boundaries (Fig. 2). Tissue-intensity curves were produced for three regions: (1) a region immediately adjacent to the injury epicenter between T1 and T2, which is immediately rostral to T2; (2) a region centered at the vertebral body of T1; and (3) a region between T1 and C7. Each region corresponded to a 150-μm-thick segment of tissue. An average hematocrit of 0.4 was used for all measurements (Hebel and Stromberg, 1986). The onset time at which contrast was seen to enter each region was manually determined, and the tissue-intensity data was fit to a curve using the DCE tool. Values for K^{trans}, the initial slope in the first 10 sec, and the peaks of the arterial and tissue curves were calculated using the Modified Tofts Model, as described above. This procedure was performed for each animal at each time point that a CT scan was obtained (t = pre-injury, 1 h post-injury, 1 day post-injury, and 7 days post-injury).

Immunohistochemistry of spinal cord sections

To compare the DCE CT technique to well-accepted immunohistochemical techniques, we used two stains to qualitatively examine blood vessel density and permeability. After the final imaging at 7 days post-injury, the animals received an overdose of sodium pentobarbital and were intracardially perfused with 4% paraformaldehyde. The spinal cords were harvested in 3-cm segments centered at the epicenter of the injury and dehydrated in 30% sucrose. The spinal cords were then frozen and sectioned at 20-μm cross-sectional thickness. To observe blood vessels, the extracellular matrix laminin was stained in regions corresponding to the regions imaged with CT. Polyclonal chicken laminin (1:500; Abcam Inc., Cambridge, MA) was applied for 24 h at 4°C with a 1% BSA and 0.2% Triton X as the blocking solution. An Alexa-Fluor 488 conjugated goat anti-chicken secondary antibody (Invitrogen, Carlsbad, CA) was added and incubated for 1 h at 37°C. To observe permeability, a fluorescein-conjugated rat IgG (Invitrogen) was used, since IgG does not cross the intact BSCB, but does permeate damaged CNS tissue. The IgG antibody was incubated for 1 h at room temperature with 10% goat serum used as a blocking solution. Cross-sections were imaged on an Olympus BX50 microscope (Olympus, Center Valley, PA) with a motorized stage at 10×magnification.

Statistical analysis

All statistics were performed using two-factorial analysis of variance (ANOVA), followed by the paired Student's t-test to compare SCBF and PS values. Differences were accepted to be statistically significant at $p < 0.05$. All errors are given as standard error of the mean.

Results

SCBF and PS measurements in the uninjured spinal cord

Initial pre-injury measurements were taken at three distinct regions in the spinal cord as a baseline comparison for all post-injury measurements. These regions were selected to investigate the hemodynamics at the epicenter of injury and two rostral regions, since the initial mechanical impact is known to have significant biochemical and hemodynamic effects for a considerable rostro-caudal distance. Since the lungs are directly ventral to the spinal cord in regions caudal to the injury, respiratory movement prevented accurate measurements in these regions. All pre-injury SCBF and PS data were averaged

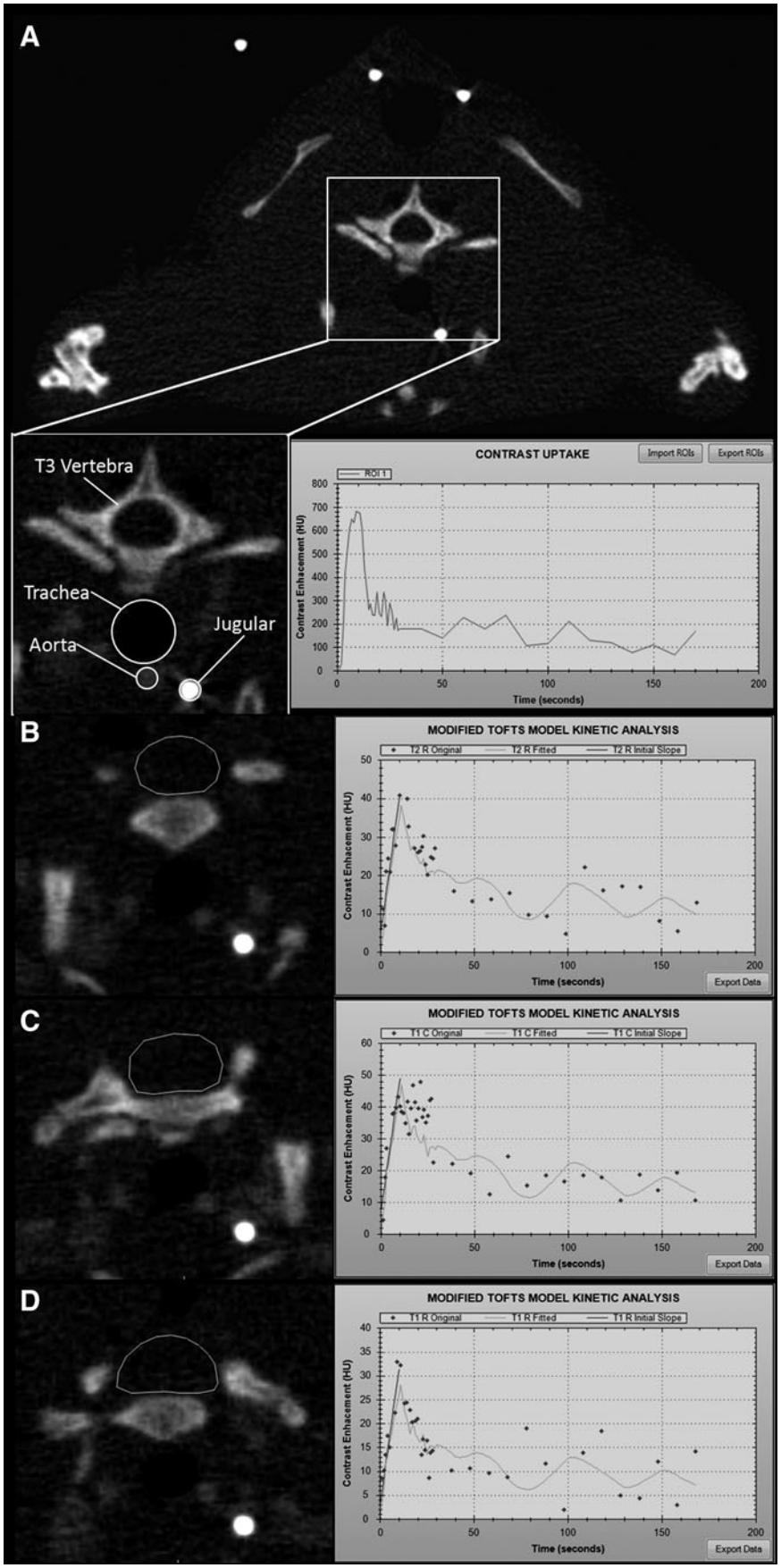
A
T3 Vertebra
Trachea
Aorta
Jugular
CONTRAST UPTAKE
Import ROIs
Export ROIs
ROI 1
Contrast Enhancement (HU)
Time (seconds)
B
MODIFIED TOFTS MODEL KINETIC ANALYSIS
T2 R Original
T2 R Fitted
T2 R Initial Slope
Contrast Enhancement (HU)
Time (seconds)
Export Data
C
MODIFIED TOFTS MODEL KINETIC ANALYSIS
T1 C Original
T1 C Fitted
T1 C Initial Slope
Contrast Enhancement (HU)
Time (seconds)
Export Data
D
MODIFIED TOFTS MODEL KINETIC ANALYSIS
T1 R Original
T1 R Fitted
T1 R Initial Slope
Contrast Enhancement (HU)
Time (seconds)
Export Data

from all animals, since treatment was not administered until post-injury. At the region nearest to the injury epicenter (T1–T2), SCBF of all groups pre-injury was 49.7 ± 1.6 mL/min/100 g. For the areas centered at T1 and T1–C7, the pre-injury means and standard error of the means were, respectively, 45.7 ± 1.6 and 45.7 ± 1.7 mL/min/100 g. These SCBF pre-injury measurements are comparable to values reported previously with the hydrogen clearance technique, for which the composite SCBF was observed to be $\sim$ 55–65 mL/min/100 g (Guha et al., 1989).

In calculating the PS value, the assumption of the model is that $K^{trans} = \text{PS}$ only when $\text{PS} << F$. However, immediately after the trauma of spinal cord compression, there is extensive hemorrhage into the extravascular space of the parenchyma, and therefore this assumption does not apply at 1 h post-injury. Thus, only pre-injury, 1-day post-injury, and 7-days post-injury PS data are reported for each of the three regions studied. The injury epicenter at T1–T2 and the region at T1 had identical pre-injury PS values of 0.32 ± 0.03 mL/min/g. At T1–C7, the pre-injury PS value was calculated at 0.25 ± 0.03 mL/min/g.

Epicenter of injury (T1–T2)

At 1 h post-injury and post-injection of treatment, there was a significant decrease in SCBF at the epicenter, to approximately 40 mL/min/100 g, for all groups (Fig. 3A). At 1 day post-injury, SCBF remained lower than pre-injury values for animals that received aCSF or HAMC, with values of 38.0 ± 3.8 and 39.1 ± 3.5 mL/min/100 g, respectively. This persistence of decreased SCBF at 1 day post-injury has been shown previously (Wu et al., 2007), and could be due to persistent leaky vasculature or destruction of vasculature at the epicenter. However, animals that received FGF2 with HAMC had a SCBF value of 47.3 ± 2.6 mL/min/100 g, which was not significantly different from pre-injury measurements. This suggests some therapeutic benefit of local release of FGF2 in HAMC (versus HAMC alone and aCSF alone), where blood flow had returned to near pre-injury values at 1 day post-injury. At 7 days post-injury, all groups had elevated SCBF values compared to pre-injury measurements; however, these were only statistically significantly higher in those animals that received FGF2 with HAMC, and not those that received either aCSF or HAMC control injections. Following this same trend, qualitative assessment of laminin staining for blood vessels at 7 days (Fig. 3C–E) showed more vessels in the area surrounding the injury for the FGF2/HAMC-treated animals (Fig. 3E and H).

At 1 day post-injury at the epicenter, PS had increased significantly for all groups, from the pre-injury measurement of 0.32 ± 0.03 mL/min/g, to comparable values of 0.48 ± 0.07 mL/min/g for the aCSF group, and 0.42 ± 0.08 mL/min/g for both the HAMC and FGF2/HAMC groups (Fig. 3B). By 7 days post-injury, the PS values had declined such that in none of the groups was it significantly higher than the pre-injury values, but animals that received FGF2 via HAMC had slightly lower PS values than controls. Immunohistochemical staining of IgG, a molecule that penetrates spinal cord tissue only when the BSCB is compromised, showed extensive staining throughout the tissue at the epicenter for all groups at 7 days post-injury (Fig. 3I–N). In support of the DCE CT method, high magnification of the tissue showed that somewhat less IgG staining was observed in the animals receiving FGF2/HAMC (Fig. 3N), compared to aCSF and HAMC controls (Fig. 3L and M, respectively).

SCBF 0.75–1 mm rostral to the injury epicenter (T1)

At 1 h post-injury and post-injection, SCBF decreased rostrally for aCSF and HAMC animals, to 38.2 ± 3.1 and 35.1 ± 4.0 mL/min/100 g, respectively (Fig. 4A). Animals that received FGF2 locally via HAMC had a SCBF of 44.1 ± 2.5 mL/min/100 g at 1 h post-injury, only 1.6 mL/min/100 g lower than the pre-injury value. At 1 day post-injury, all groups showed some improvement in SCBF, although FGF2-treated animals had values most similar to their pre-injury measurements. As was observed at the epicenter, higher SCBF values were observed at 7 days post-injury for the FGF2/HAMC-treated group, compared to pre-injury measurements. A trend toward higher SCBF was also observed for HAMC alone in this region. The aCSF group, however, only returned to pre-injury values, and did not show higher reperfusion rates at T1. At 7 days post-injury, greater vessel density was seen with laminin staining in the cords for the FGF2/HAMC-treated animals compared to both the aCSF and HAMC animals (Fig. 4E and H).

PS values rostral to the injury were moderately increased at 1 day post-injury relative to pre-injury measurements (Fig. 4B), with smaller changes seen here than those at the epicenter. Animals that received FGF2 via HAMC showed a marginal increase of only 0.02 mL/min/g, compared to the increases seen in the aCSF and HAMC groups, which rose by 0.11 and 0.12 mL/min/g, respectively. At 7 days post-injury, the values in the aCSF-treated animals remained higher than their pre-injury values, and animals that received HAMC alone showed reductions in PS nearly to pre-injury levels. This was also observed with IgG staining, where less staining was seen in animals that received HAMC than in those receiving aCSF (Fig. 4M and L, respectively). Additionally, IgG staining for FGF2/HAMC-treated animals showed less than that in both control groups (Fig. 4N). This was substantiated by DCE CT, for which the PS values seen at 7 days were the lowest in animals that received FGF2/HAMC.

FIG. 2. **(A)** Representative arterial region of interest at T3, where a cross-section of the entire rat is shown. The box outlines the inset below showing anatomical landmarks, including the contrast-filled catheter inside the jugular vein, the aorta (used for determining the arterial input function), the trachea, and the intact T3 vertebra. The corresponding arterial input function taken from this region is shown to the right of the inset. **(B)** A representative region of interest near the injury epicenter (T1–T2), and the corresponding tissue uptake curve at right. Note that the spinous process and laminae have been removed in **B**, **C**, and **D**, and that the vertebral body is still present below the outlined region of interest. **(C)** A representative region of interest 0.75–1 mm rostral to the epicenter (T1), where a laminectomy was performed, and the corresponding tissue uptake curve. **(D)** A representative region of interest 1.8–2 mm rostral to the epicenter (T1–C7), and the corresponding tissue uptake curve.

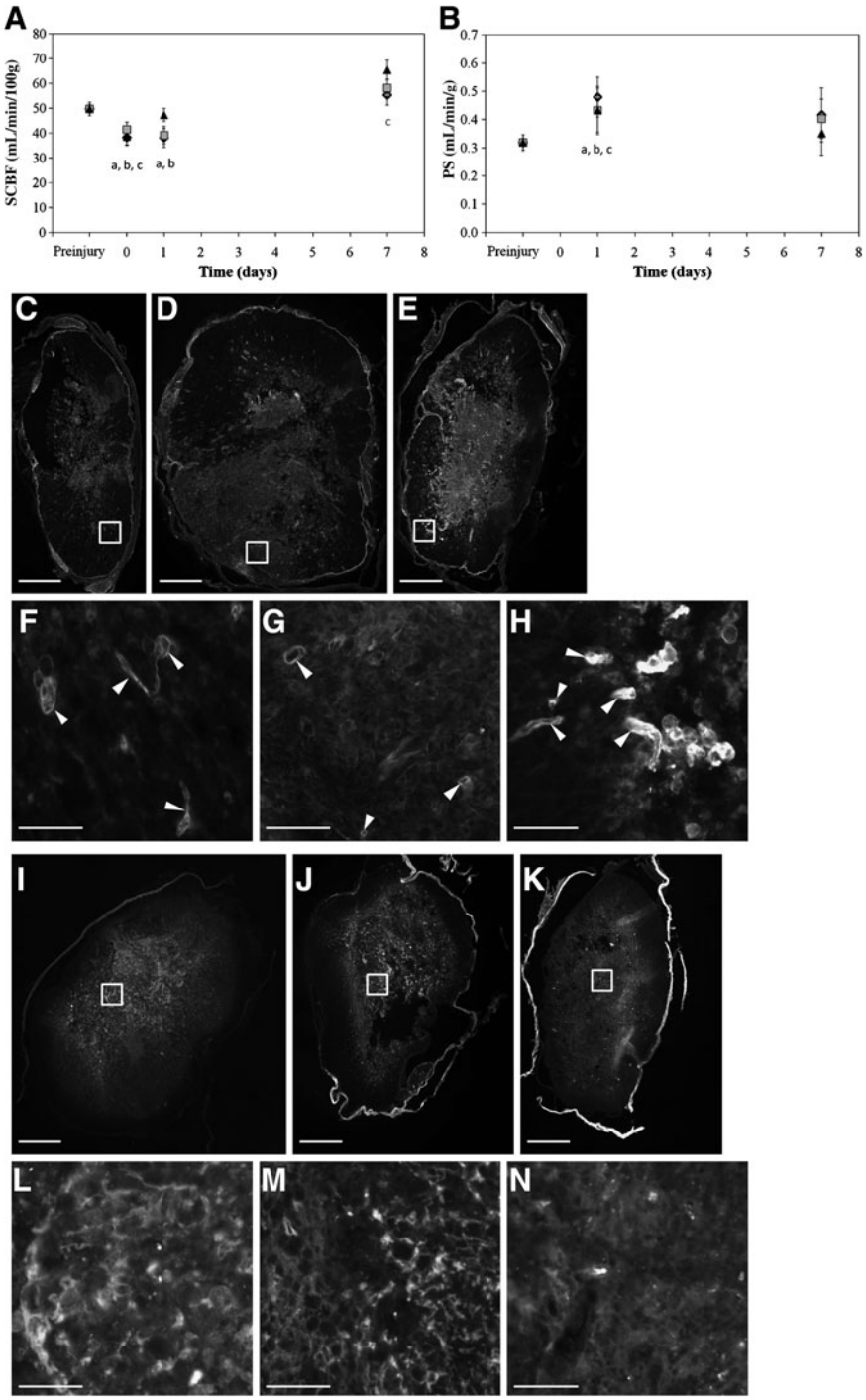

FIG. 3. Near the epicenter of injury at T1–T2, DCE CT was used to measure: **(A)** spinal cord blood flow (SCBF), and **(B)** permeability-surface (PS) area products for animals receiving: FGF2/HAMC (triangles), aCSF (diamonds), and HAMC (squares) ($n = 8$, mean $\pm$ standard error of the mean are shown; letters indicate statistically significant differences [$p < 0.05$] compared to pre-injury values: a, aCSF; b, HAMC; c, FGF2/HAMC). Images **C**, **D**, and **E** show representative spinal cord cross-sections with laminin staining for aCSF-, HAMC-, and FGF2/HAMC-treated animals, with the areas in the white boxes shown at higher magnification below, in images **F**, **G**, and **H**. White arrowheads indicate blood vessels in the magnified areas. Images **I**, **J**, and **K** are representative images of spinal cords with IgG staining for the aCSF, HAMC, and FGF2/HAMC groups, with the areas in the white boxes shown below at higher magnification in images **L**, **M**, and **N** (scale bars in **C**–**E** and **I**–**K** = 1 mm, and the bars in **F**–**H** and **L**–**N** = 100 μm; aCSF, artificial cerebrospinal fluid; HAMC, hyaluronan and methylcellulose; FGF2, fibroblast growth factor 2).

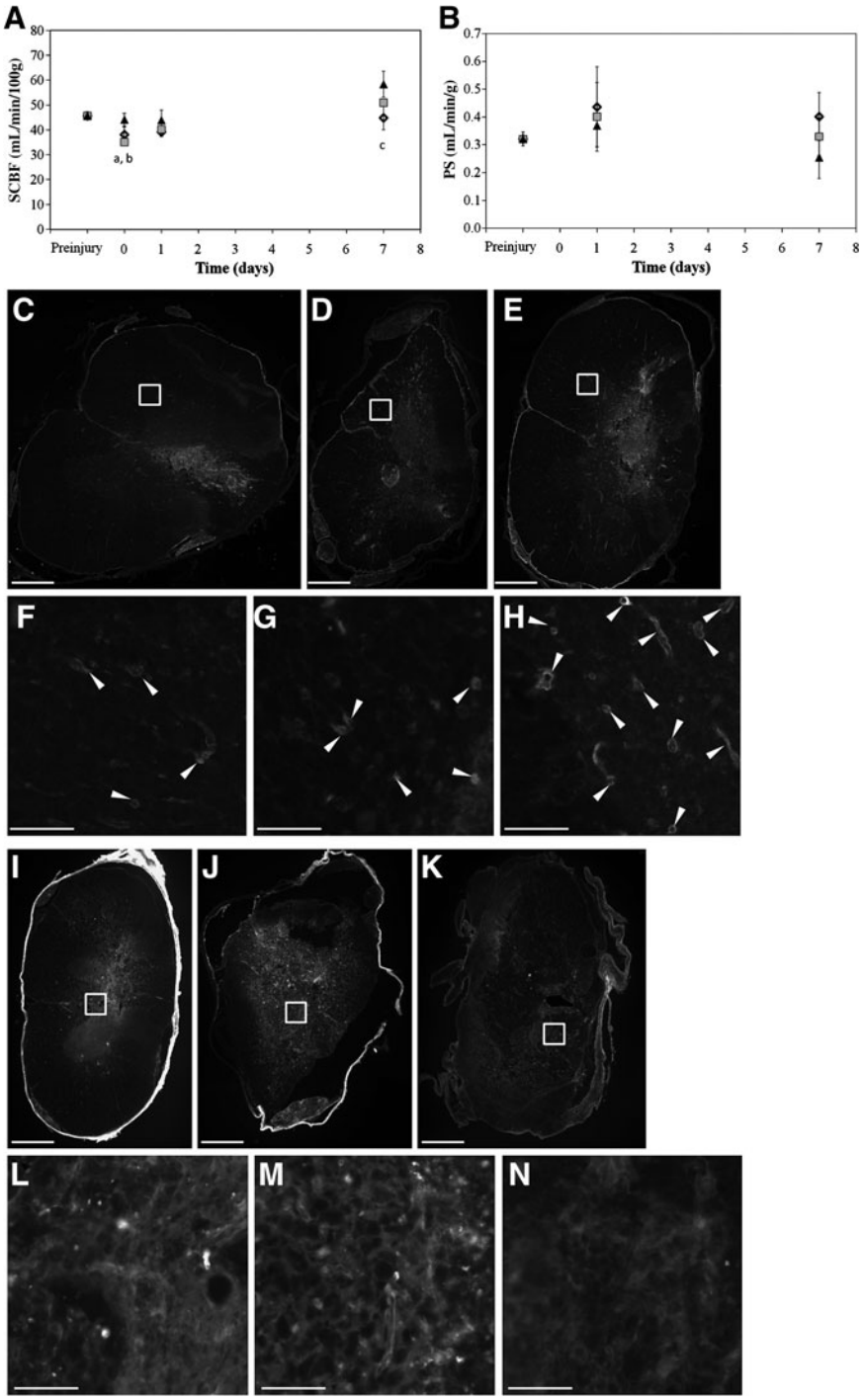

FIG. 4. Dynamic contrast enhancement computed tomography at 0.75–1 mm rostral to the epicenter at T1 was used to obtain **(A)** spinal cord blood flow (SCBF), and **(B)** permeability-surface (PS) area measurements for animals receiving: FGF2/HAMC (triangles), aCSF (diamonds), and HAMC (squares) ($n = 8$; mean ± standard error of the mean are shown; letters indicate statistical differences as compared to pre-injury values: a, aCSF; b, HAMC; c, FGF2/HAMC). Images **C**, **D**, and **E** show representative spinal cord cross sections with laminin staining for aCSF-, HAMC-, and FGF2/HAMC-treated animals, with the areas in the white boxes shown at higher magnification below in images **F**, **G**, and **H**. White arrowheads indicate blood vessels in the magnified areas. Images **I**, **J**, and **K** are representative images of spinal cords with IgG staining for aCSF, HAMC, and FGF2/HAMC, with the areas in the white boxes shown below at higher magnification in images **L**, **M**, and **N** (scale bars in **C**–**E** and **I**–**K** = 1 mm, and the bars in **F**–**H** and **L**–**N** = 100 μm; aCSF, artificial cerebrospinal fluid; HAMC, hyaluronan and methylcellulose; FGF2, fibroblast growth factor 2).

SCBF 1.8–2 mm rostral to the injury epicenter (T1–C7)

As far as 2 mm away from the injury epicenter, at T1–C7, SCBF decreased significantly from the pre-injury measurement of 45.7 ± 1.7 mL/min/100 g for all groups at 1 h post-injury, to values of 38.2 ± 3.4, 36.3 ± 3.1, and 36.5 ± 1.6 mL/min/100 g for the aCSF, HAMC, and FGF2/HAMC groups, respectively. At 1 day post-injury, all groups had increased to values that were lower, but were not significantly different from pre-injury values. At 7 days post-injury, higher reperfusion rates were observed for all groups, similarly to the findings at the epicenter and T1 regions. The aCSF- and HAMC-treated groups increased to 49.3 ± 2.4 and 53.5 ± 5.1 mL/min/100 g, respectively. In this region at 7 days, SCBF in animals that received FGF2 treatment was 60.9 ± 3.5 mL/min/100 g, which was significantly higher than both pre-injury values and aCSF controls. Laminin staining also qualitatively showed improved blood vessel density in FGF2/HAMC animals relative to aCSF animals (Fig. 5H and F, respectively).

At 1 day post-injury, the PS value for the FGF2/HAMC-treated group was 0.28 ± 0.10 mL/min/g, which was similar to the pre-injury value of 0.25 ± 0.03 mL/min/g, whereas the PS values for both the aCSF and HAMC groups were higher, with values of 0.42 ± 0.08 and 0.37 ± 0.10 mL/min/g, respectively. At 7 days post-injury, the PS values of all groups had decreased, and FGF2/HAMC-treated animals showed the greatest decrease in PS values, to 0.18 ± 0.05 mL/min/g, followed by HAMC-treated animals, which had a PS level of 0.28 ± 0.07 mL/min/g, which was similar to pre-injury values, and then aCSF-treated animals, which had PS values of 0.36 ± 0.03 mL/min/g. The FGF2/HAMC treatment showed significantly lower PS values than aCSF-treated animals at this time point. This was also observed with IgG immunohistochemistry, as shown in Figure 5C–E, that less IgG penetrated into the tissue in the FGF2/HAMC-treated animals. The reduction in PS and increase in SCBF observed with FGF2 delivery further supports the hypothesis that early delivery of FGF2 has prolonged effects on tissue recovery. Additionally, the decreases in PS and IgG staining relative to aCSF animals for those receiving HAMC alone suggests a therapeutic benefit of HAMC, which is consistent with previous reports (Gupta et al., 2006).

Discussion

Here, for the first time, dynamic perfusion CT was utilized to serially measure SCBF and PS of the uninjured and injured rat spinal cord. Controls showed the characteristic drop in SCBF that has been observed using other methods (Guha et al., 1989; Wu et al., 2007), and the spontaneous recovery that occurs within 7 days, a period in which spontaneous angiogenesis is thought to occur (Loy et al., 2002). Although SCBF measurements at 7 days were higher than pre-injury measurements, significant tissue degeneration had still occurred at the epicenter for all groups. Laminin staining for the extracellular matrix surrounding blood vessels at 7 days post-injury showed that those vessels on the periphery of the cord were better preserved than those in the center (Fig. 3C–E). Also, the large vessels on the surface of the cord, such as the anterior spinal artery and vein, were preserved, even at the epicenter. These larger vessels are likely to contribute more substantially to the SCBF measurements made with DCE CT than small capillaries; however, the increase in SCBF above pre-injury levels could be a result of both persistent vasodilation of the larger peripheral vessels, as well as an increase in the density of small vessels in the parenchyma. PS increased following injury, as has previously been shown (Noble and Wrathall, 1989; Popovich et al., 1996), and to some extent was attenuated over time, although it remained higher than pre-injury values at regions nearest to the site of injury. Staining with IgG, a molecule that does not cross the intact BSCB, was used to qualitatively compare to the PS measurements obtained with DCE CT at 7 days post-injury. This immunohistochemical assessment showed similar trends to the CT data, thus validating this technique for permeability measurements in the spinal cord. However, it is important to note that permeability is related to the size of the molecule used in the assessment; thus these data showing permeability attenuating within 7 days post-injury cannot be directly compared to previous permeability studies, that showed longer-term permeability using smaller molecules. Future optimization of CT resolution will greatly improve the ability to differentiate between gray matter and white matter measurements, and will allow us to further probe the mechanisms by which FGF2 and other molecules may affect blood flow. Notwithstanding the variability seen in the CT measurements, the results reported here suggest that dynamic CT is an effective tool with which to study SCBF and permeability, and that it has the advantages of being minimally-invasive and repeatable in the same animal.

Immediately following SCI, several vascular changes occur at the site of injury. Grossly-injured vessels leak blood and fluid into the parenchyma of the tissue, leading to edema. This leads to a disruption of the BSCB, since cells and proteins normally absent in the spinal cord consequently accumulate in the tissue. To seal burst blood vessels and limit hemorrhage, widespread vasoconstriction occurs, thus lowering blood flow to the area. However, this global vasoconstriction leads to ischemia in the surrounding tissue penumbra. Systemic FGF2 infusion causes vasodilation *in vivo*, by opening ATP-sensitive potassium channels and enhancing the release of nitric oxide (Cuevas et al., 1991; Ziche and Morbidelli, 2000).

In the experiments performed here, localized delivery of FGF2 via HAMC raised SCBF to near pre-injury values at the injury epicenter and at two rostral sites for the first 24 h post-injury. The immediate delivery of FGF2 via HAMC into the intrathecal space may cause vasodilation of the large peripheral vessels on the surface of the cord, potentially leading to this stabilization of blood flow very early in the secondary injury process. *In vivo* angiogenesis requires persistent vasodilation, which allows existing vessels to expand into poorly vascularized tissue (Ziche and Morbidelli, 2000). Previously we showed that FGF2 delivered locally via HAMC was observed to diffuse into the spinal cord in 5- to 50-ng/mL concentrations, which have been used to stimulate angiogenesis *in vitro*, for up to 6 h (Kang et al., 2009b); this localized delivery may have contributed to the higher perfusion rates seen at 7 days post-injury at all three tissue sites, where FGF2 concentrations sustained over several hours within the cord could have persistently dilated even small vessels, thereby stimulating angiogenic pathways and increasing blood flow relative to controls. At the epicenter at 1 day post-injury, SCBF showed a slight increase in the animals in the FGF2/HAMC

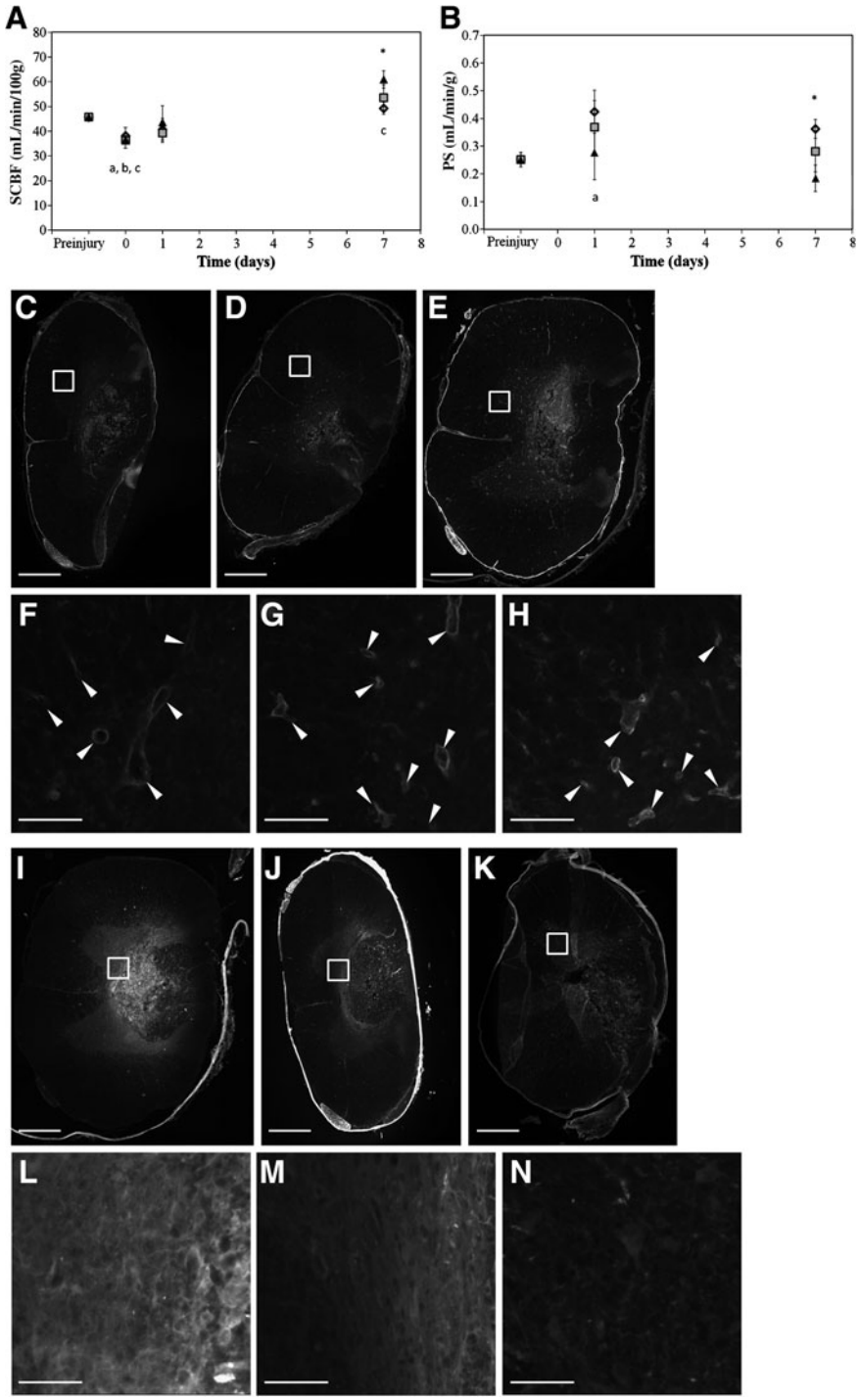

FIG. 5. Dynamic contrast enhancement computed tomography at 1.8–2 mm rostral to the epicenter at T1–C7 was used to obtain **(A)** spinal cord blood flow (SCBF), and **(B)** permeability-surface (PS) area measurements for animals receiving: FGF2/HAMC (triangles), aCSF (diamonds), and HAMC (squares) ($n = 8$; mean ± standard error of the mean are shown; letters indicate statistical differences as compared to pre-injury values: a, aCSF; b, HAMC; c, FGF2/HAMC; the asterisks indicate statistical significance between the aCSF and FGF2/HAMC groups at that time point). Images **C**, **D**, and **E** show representative spinal cord cross sections with laminin staining for aCSF-, HAMC-, and FGF2/HAMC-treated animals, with the areas in the white boxes shown at higher magnification below in images **F**, **G**, and **H**. White arrowheads indicate blood vessels in the magnified areas. Images **I**, **J**, and **K** are representative images of spinal cords with IgG staining for the aCSF, HAMC, and FGF2/HAMC groups, with the areas in the white boxes shown below at higher magnification in images **L**, **M**, and **N** (scale bars in **C**–**E** and **I**–**K** = 1 mm, and the bars in **F**–**H** and **L**–**N** = 100 μm; aCSF, artificial cerebrospinal fluid; HAMC, hyaluronan and methylcellulose; FGF2, fibroblast growth factor 2).

group, but permeability was the same for all groups at this time point. The process of angiogenesis creates leaky vasculature initially, but FGF2 is known to promote maturation of newly-formed vessels (Murakami and Simons, 2008). Since permeability did not decrease at 1 day in the FGF2-treated animals, but SCBF did increase, it is possible that FGF2 stimulated the formation of small vessels. At 7 days, these new vessels promoted by FGF2 at 1 day post-injury may have matured, thus contributing to the reduced PS and the significant increase in SCBF seen in this group. Moreover, FGF2 may directly stimulate angiogenesis by inducing endothelial proliferation, or stimulating expression of VEGF (Seghezzi et al., 1998), or nitric oxide (Ziche and Morbidelli, 2000), in endothelial cells and astrocytes, respectively, to regulate angiogenesis. While the mechanism is not well understood, it is clear that notwithstanding the brief period of FGF2 delivery following SCI, long-lasting benefits were observed for SCBF after its localized delivery via HAMC.

The control injections of HAMC and aCSF showed a characteristic decrease in SCBF within the first hour, which remained lower than pre-injury values at 24 h. Blood flow at 7 days for these controls showed that SCBF returned to pre-injury levels, although the HAMC animals showed a statistically insignificant trend toward greater reperfusion. HA is a large molecule, but it is easily hydrolyzed and is also broken down by free radicals (Presti and Scott, 1994), which cause tissue damage and are present after SCI. HA may provide an early protective effect by scavenging free radicals. Subsequently, the fragments of HA could cross the damaged pia after SCI to promote angiogenesis, as has been demonstrated in wound healing by upregulating collagen production in endothelial cells (Lees et al., 1995; West and Kumar, 1989). HA has been seen to diffuse out of the HAMC gel within 24 h after injection (Kang et al., 2009a), although a significant improvement in locomotor function was observed at 7 days post-injury for rats injected with HAMC relative to aCSF controls (Gupta et al., 2006). The limited benefit of HAMC alone seen here for SCBF rostral to the epicenter of injury may have contributed to the improved functional behavior previously reported. Taken together, these results suggest that HAMC itself may have an angiogenic effect on the tissue, which may be enhanced by the addition of FGF2.

Disruption of the BSCB occurs rapidly at the site of injury due to mechanical insult, and the downstream biochemical pathways lead to similar disturbances in the areas surrounding the injury. The tight junctions between endothelial cells that line blood vessels and normally effectively block passive transport of large molecules across the BSCB into the parenchyma (Reese and Karnovsky, 1967) are disrupted by injury, allowing uncontrolled extravasation of plasma proteins (Noble and Wrathall, 1989). The BSCB remains permeable to very small molecules for at least 28 days after SCI (Popovich et al., 1996), although for larger molecules, the barrier is restored at 14 days (Noble and Wrathall, 1989). Increased permeability of the BSCB has been observed in several vertebral segments away from the epicenter of injury (Noble and Wrathall, 1989; Popovich et al., 1996), suggesting a widespread biochemical mechanism. FGF2 has been shown to play a role in the BSCB, where tight junction proteins are preserved in organotypic cortical slices when exposed to FGF2 in the surrounding media (Bendfeldt et al., 2007). Moreover, the tight junction proteins occludin and zona occludens-1 were reduced in FGF2-knockout mice (Reuss et al., 2003), suggesting a role for FGF2 in the regulation of these proteins. FGF2 signaling has also been shown to mediate signaling between astrocytes and endothelial cells during angiogenesis (Abbott et al., 2006), and these interactions are also necessary for functioning of the BSCB (Beck et al., 1984; Hayashi et al., 1997). HAMC alone showed a trend toward reducing PS values at regions rostral to the epicenter of injury, and localized delivery of FGF2 via HAMC restored PS nearly to pre-injury values in these same regions at 1 day post-injury. At 7 days post-injury, the PS values were lower than pre-injury values, and were significantly lower in animals treated with FGF2/HAMC than in those treated with aCSF, in the region most rostral to the epicenter, at T1–C7. These data also support the hypothesis that short-term delivery of FGF2 via HAMC can have a long-term impact on tissue recovery.

Here we have shown that SCBF measurements at three distinct regions of the spinal cord show characteristic patterns of recovery using dynamic perfusion CT imaging. Localized delivery of FGF2 via HAMC stabilized SCBF, nearly to pre-injury values, and also caused increased perfusion at 7 days post-injury, compared to pre-injury measurements. PS measurements indicated a characteristic increase in permeability at 1 day following injury. Delivery of FGF2 with HAMC stabilized PS at regions rostral to the epicenter of injury, with significantly lower PS values than those in aCSF controls at 7 days in the region most rostral to the epicenter at T1–C7. HAMC alone also showed a moderate improvement in PS at regions distal to the epicenter, supporting previous data that the delivery vehicle itself may have therapeutic benefit. Importantly, we report here that dynamic perfusion CT is a valid method for serially measuring SCBF and permeability after SCI in small animals, and that FGF2 delivered locally via HAMC can improve SCBF and permeability following SCI.

Acknowledgments

The authors are indebted to Peter Poon for all of his surgical and technical assistance with these studies. The authors would also like to thank Sunmo Kim and Nicolas Gonzalez for fruitful discussions regarding perfusion CT modeling and measurements. We acknowledge funding from the Canadian Institute for Health Research (to M.S.S. and C.H.T.).

Author Disclosure Statement

No competing financial interests exist.

References

Abbott, N.J., Ronnback, L., and Hansson, E. (2006). Astrocyte-endothelial interactions at the blood-brain barrier. Nat. Rev. Neurosci. 7, 41–53.

Beck, D.W., Vinters, H.V., Hart, M.N., and Cancilla, P.A. (1984). Glial cells influence polarity of the blood-brain barrier. J. Neuropathol. Exp. Neurol. 43, 219–224.

Bendfeldt, K., Radojevic, V., Kapfhammer, J., and Nitsch, C. (2007). Basic fibroblast growth factor modulates density of blood vessels and preserves tight junctions in organotypic cortical cultures of mice: a new in vitro model of the blood-brain barrier. J. Neurosci. 27, 3260–3267.

Bisdas, S., Rumboldt, Z., Surlan, K., Koh, T.S., Deveikis, J., and Spampinato, M.V. (2008). Perfusion CT measurements in healthy cervical spinal cord: feasibility and repeatability of the

study as well as interchangeability of the perfusion estimates using two commercially available software packages. Eur. Radiol. 18, 2321–2328.

Cuevas, P., Carceller, F., Ortega, S., Zazo, M., Nieto, I., and Gimenez-Gallego, G. (1991). Hypotensive activity of fibroblast growth factor. Science 254, 1208–1210.

Fehlings, M.G. (2001). Editorial: recommendations regarding the use of methylprednisolone in acute spinal cord injury: making sense out of the controversy. Spine 26, S56–S57.

Guha, A., Tator, C.H., and Rochon, J. (1989). Spinal cord blood flow and systemic blood pressure after experimental spinal cord injury in rats. Stroke 20, 372–377.

Gupta, D., Tator, C.H., and Shoichet, M.S. (2006). Fast-gelling injectable blend of hyaluronan and methylcellulose for intrathecal, localized delivery to the injured spinal cord. Biomaterials 27, 2370–2379.

Hawryluk, G.W., Rowland, J., Kwon, B.K., and Fehlings, M.G. (2008). Protection and repair of the injured spinal cord: a review of completed, ongoing, and planned clinical trials for acute spinal cord injury. Neurosurg Focus 25, E14.

Hayashi, Y., Nomura, M., Yamagishi, S., Harada, S., Yamashita, J., and Yamamoto, H. (1997). Induction of various blood-brain barrier properties in non-neural endothelial cells by close apposition to co-cultured astrocytes. Glia 19, 13–26.

Hebel, R., and Stromberg, M.W. (1986). *Anatomy and Embryology of the Laboratory Rat*. BioMed Verlag: Worthsee.

Jimenez Hamann, M.C., Tsai, E.C., Tator, C.H., and Shoichet, M.S. (2003). Novel intrathecal delivery system for treatment of spinal cord injury. Exp. Neurol. 182, 300–309.

Jones, L.L. and Tuszynski, M.H. (2001). Chronic intrathecal infusions after spinal cord injury cause scarring and compression. Microsc. Res. Tech. 54, 317–324.

Kang, C.E., Poon, P.C., Tator, C.H., and Shoichet, M.S. (2009a). A new paradigm for local and sustained release of therapeutic molecules to the injured spinal cord for neuroprotection and tissue repair. Tissue Eng. Part A 15, 595–604.

Kang, C.E., Tator, C.H., and Shoichet, M.S. (2009b). Conjugation of poly(ethylene glycol) to fibroblast growth factor 2 enhances distribution in spinal cord tissue. J. Controlled Release, in press.

Kety, S.S., and Schmidt, C.F. (1948). The nitrous oxide method for the quantitative determination of cerebral blood flow in man; theory, procedure and normal values. J. Clin. Invest. 27, 476–483.

Kety, S.S. (1951). The theory and applications of the exchange of inert gas at the lungs and tissues. Pharmacol. Rev. 3, 1–41.

Lees, V.C., Fan, T.P., and West, D.C. (1995). Angiogenesis in a delayed revascularization model is accelerated by angiogenic oligosaccharides of hyaluronan. Lab. Invest. 73, 259–266.

Lee, T.T., Green, B.A., Dietrich, W.D., and Yezierski, R.P. (1999). Neuroprotective effects of basic fibroblast growth factor following spinal cord contusion injury in the rat. J. Neurotrauma 16, 347–356.

Leggett, D.A., Miles, K.A., and Kelley, B.B. (1998). Blood-brain barrier and blood volume imaging of cerebral glioma using functional CT: a pictorial review. Australas. Radiol. 42, 335–340.

Loy, D.N., Crawford, C.H., Darnall, J.B., Burke, D.A., Onifer, S.M., and Whittemore, S.R. (2002). Temporal progression of angiogenesis and basal lamina deposition after contusive spinal cord injury in the adult rat. J. Comp. Neurol. 445, 308–324.

Miles, K.A., Charnsangavej, C., Lee, F.T., Fishman, E.K., Horton, K., and Lee, T.Y. (2000). Application of CT in the investigation of angiogenesis in oncology. Acad. Radiol. 7, 840–850.

Miles, K.A., Hayball, M.P., and Dixon, A.K. (1993). Functional images of hepatic perfusion obtained with dynamic CT. Radiology 188, 405–411.

Miles, K.A., Leggett, D.A., Kelley, B.B., Hayball, M.P., Sinnatamby, R., and Bunce, I. (1998). In vivo assessment of neovascularization of liver metastases using perfusion CT. Br. J. Radiol. 71, 276–281.

Miles, K.A. (1991). Measurement of tissue perfusion by dynamic computed tomography. Br. J. Radiol. 64, 409–412.

Montesano, R., Vassalli, J.D., Baird, A., Guillemin, R., and Orci, L. (1986). Basic fibroblast growth factor induces angiogenesis in vitro. Proc. Natl. Acad. Sci. USA 83, 7297–7301.

Murakami, M., and Simons, M. (2008). Fibroblast growth factor regulation of neovascularization. Curr. Opin. Hematol. 15, 215–220.

Noble, L.J., and Wrathall, J.R. (1989). Distribution and time course of protein extravasation in the rat spinal cord after contusive injury. Brain Res. 482, 57–66.

Nozaki, K., Finklestein, S.P., and Beal, M.F. (1993). Basic fibroblast growth factor protects against hypoxia-ischemia and NMDA neurotoxicity in neonatal rats. J. Cereb. Blood Flow Metab. 13, 221–228.

Peters, A.M., Brown, J., Hartnell, G.G., Myers, M.J., Haskell, C., and Lavender, J.P. (1987a). Non-invasive measurement of renal blood flow with 99mTc DTPA: comparison with radiolabelled microspheres. Cardiovasc. Res. 21, 830–834.

Peters, A.M., Gunasekera, R.D., Henderson, B.L., Brown, J., Lavender, J.P., De Souza, M., Ash, J. M., and Gilday, D.L. (1987b). Noninvasive measurement of blood flow and extraction fraction. Nucl. Med. Commun. 8, 823–837.

Popovich, P.G., Horner, P.J., Mullin, B.B., and Stokes, B.T. (1996). A quantitative spatial analysis of the blood-spinal cord barrier. I. Permeability changes after experimental spinal contusion injury. Exp. Neurol. 142, 258–275.

Presti, D., and Scott, J.E. (1994). Hyaluronan-mediated protective effect against cell damage caused by enzymatically produced hydroxyl (OH.) radicals is dependent on hyaluronan molecular mass. Cell Biochem. Funct. 12, 281–288.

Rabchevsky, A.G., Fugaccia, I., Fletcher-Turner, A., Blades, D.A., Mattson, M.P., and Scheff, S.W. (1999). Basic fibroblast growth factor (bFGF) enhances tissue sparing and functional recovery following moderate spinal cord injury. J. Neurotrauma 16, 817–830.

Rabchevsky, A.G., Fugaccia, I., Turner, A.F., Blades, D.A., Mattson, M.P., and Scheff, S.W. (2000). Basic fibroblast growth factor (bFGF) enhances functional recovery following severe spinal cord injury to the rat. Exp. Neurol. 164, 280–291.

Reese, T.S., and Karnovsky, M.J. (1967). Fine structural localization of a blood-brain barrier to exogenous peroxidase. J. Cell Biol. 34, 207–217.

Reeve Foundation, C.D. (2009). One Degree of Separation: Paralysis and Spinal Cord Injury in the United States. Retrieved January 14, 2010, from http://www.christopherreeve.org/site/c.mtKZKgMWKwG/b.5184189/k.5587/Paralysis_Facts__Figures.htm.

Relf, M., LeJeune, S., Scott, P.A., Fox, S., Smith, K., Leek, R., Moghaddam, A., Whitehouse, R., Bicknell, R., and Harris, A.L. (1997). Expression of the angiogenic factors vascular endothelial cell growth factor, acidic and basic fibroblast growth factor, tumor growth factor beta-1, platelet-derived endothelial cell growth factor, placenta growth factor, and pleiotrophin in human primary breast cancer and its relation to angiogenesis. Cancer Res. 57, 963–969.

Reuss, B., Dono, R., and Unsicker, K. (2003). Functions of fibroblast growth factor (FGF)-2 and FGF-5 in astroglial differentiation and blood-brain barrier permeability: evidence from mouse mutants. J. Neurosci. 23, 6404–6412.

Rivlin, A.S., and Tator, C.H. (1978). Effect of duration of acute spinal cord compression in a new acute cord injury model in the rat. Surg. Neurol. 10, 38–43.

Sandler, A.N., and Tator, C.H. (1976). Review of the measurement of normal spinal cord blood flow. Brain Res. 118, 181–198.

Seghezzi, G., Patel, S., Ren, C.J., Gualandris, A., Pintucci, G., Robbins, E.S., Shapiro, R.L., Galloway, A.C., Rifkin, D.B., and Mignatti, P. (1998). Fibroblast growth factor-2 (FGF-2) induces vascular endothelial growth factor (VEGF) expression in the endothelial cells of forming capillaries: an autocrine mechanism contributing to angiogenesis. J. Cell Biol. 141, 1659–1673.

Shing, Y., Folkman, J., Haudenschild, C., Lund, D., Crum, R., and Klagsbrun, M. (1985). Angiogenesis is stimulated by a tumor-derived endothelial cell growth factor. J. Cell Biochem. 29, 275–287.

Tateishi, U., Nishihara, H., Watanabe, S., Morikawa, T., Abe, K., and Miyasaka, K. (2001). Tumor angiogenesis and dynamic CT in lung adenocarcinoma: radiologic-pathologic correlation. J. Comput. Assist. Tomogr. 25, 23–27.

Tator, C.H. (2006). Review of treatment trials in human spinal cord injury: issues, difficulties, and recommendations. Neurosurgery 59, 957–982; discussion 982–987.

Toda, H., Maruyama, H., Budgell, B., and Kurosawa, M. (2008). Responses of dorsal spinal cord blood flow to noxious mechanical stimulation of the skin in anesthetized rats. J. Physiol. Sci. 58, 263–270.

Tofts, P.S., Brix, G., Buckley, D.L., Evelhoch, J.L., Henderson, E., Knopp, M.V., Larsson, H.B., Lee, T.Y., Mayr, N.A., Parker, G.J., Port, R.E., Taylor, J., and Weisskoff, R.M. (1999). Estimating kinetic parameters from dynamic contrast-enhanced T(1)-weighted MRI of a diffusable tracer: standardized quantities and symbols. J. Magn. Reson. Imaging 10, 223–232.

West, D.C., and Kumar, S. (1989). The effect of hyaluronate and its oligosaccharides on endothelial cell proliferation and monolayer integrity. Exp. Cell Res. 183, 179–196.

Wu, X.H., Yang, S.H., Duan, D.Y., Cheng, H.H., Bao, Y.T., and Zhang, Y. (2007). Anti-apoptotic effect of insulin in the control of cell death and neurologic deficit after acute spinal cord injury in rats. J. Neurotrauma 24, 1502–1512.

Yeung, W.T., Lee, T.Y., Del Maestro, R.F., Kozak, R., Bennett, J., and Brown, T. (1994). Effect of steroids on iopamidol blood-brain transfer constant and plasma volume in brain tumors measured with X-ray computed tomography. J. Neurooncol. 18, 53–60.

Yi, C.A., Lee, K.S., Kim, E.A., Han, J., Kim, H., Kwon, O.J., Jeong, Y.J., and Kim, S. (2004). Solitary pulmonary nodules: dynamic enhanced multi-detector row CT study and comparison with vascular endothelial growth factor and microvessel density. Radiology 233, 191–199.

Ziche, M., and Morbidelli, L. (2000). Nitric oxide and angiogenesis. J. Neurooncol. 50, 139–148.

Address correspondence to:
Molly S. Shoichet, Ph.D.
The Donnelly Centre
160 College Street
Room 514
Toronto, Ontario, Canada M5S 3E1

E-mail: molly.shoichet@utoronto.ca